

Soft-Switched CCM Boost Converters With High Voltage Gain for High-Power Applications

Sungsik Park and Sewan Choi, *Senior Member, IEEE*

Abstract—This paper proposes a new soft-switched continuous-conduction-mode (CCM) boost converter suitable for high-power applications such as power factor correction, hybrid electric vehicles, and fuel cell power conversion systems. The proposed converter achieves zero-voltage-switched (ZVS) turn-on of active switches in CCM and zero-current-switched turn-off of diodes leading to negligible reverse-recovery loss. The components' voltage ratings and energy volumes of passive components of the proposed converter are greatly reduced compared to the conventional zero-voltage-transition converter. Voltage conversion ratio is almost doubled compared to the conventional boost converter. Extension of the proposed concept to realize multiphase dc-dc converters is discussed. Experimental results from a 1.5-kW prototype are provided to validate the proposed concept.

Index Terms—Continuous conduction mode (CCM), high-power applications, high voltage gain, nonisolated, soft switched.

I. INTRODUCTION

CONTINUOUS-conduction-mode (CCM) boost converters have been widely used as the front-end converter for active input current shaping [6]. In recent years, CCM boost converters are increasingly needed in high-power applications such as hybrid electric vehicles and fuel cell power conversion systems. High power density and high efficiency are major concerns in high-power CCM boost converters [1], [7].

The hard-switched CCM boost converter suffers from severe diode reverse-recovery problem in high-current high-power applications. That is, when the main switch is turned on, a shoot-through of the output capacitor to ground due to the diode reverse recovery causes a large current spike through the diode and main switch. This not only incurs significant turn-off loss of the diode and turn-on loss of the main switch, but also causes severe electromagnetic interference (EMI) emission. The effect of the reverse-recovery-related problems become more significant for high switching frequency at high power level. Therefore, the hard-switched CCM boost converter is not capable to achieve high efficiency and high power density at high power level.

Many soft-switching techniques on CCM boost converters have been proposed [2]–[4], [6], [8]–[10]. The zero-voltage-switched (ZVS) quasiresonant converter (QRC) achieves soft

switching of the main switch with ZVS and the diode with zero current switched (ZCS), but both main switch and diode suffer from an excessive voltage stress due to resonant operation. The ZVS quasquare-wave converter (QSW) technique offers ZVS turn-on for both main switch and diode without increasing their voltage stresses. However, both main switch and diode suffer from a high current stress resulting in significant conduction losses. Furthermore, turn-off loss of the main switch is considerable. Since both ZVS-QRC and ZVS-QSW techniques achieve soft switching only at the expense of increased conduction losses due to voltage or current stresses of the components, they are not suitable for high-power applications [10].

The zero-voltage-transition (ZVT) pulsewidth modulation (PWM) converter [10] achieves soft switching of the main switch and diode without increasing their voltage or current stresses, since ZVS is achieved by partial resonance of the shunt branch across the main switch. Furthermore, the reverse-recovery-related problem is alleviated by controlling diode current decrease rate di/dt during its turn off. However, severe undesired resonance may occur in the shunt branch. Adding a rectifier and saturable inductor can mitigate the resonance, but this causes circuit complexity and additional cost [5]. Also, the auxiliary switch in the shunt branch is hard switched, and the duty ratio of the auxiliary switch limits the effective duty ratio of the main switch, leading to decreased voltage conversion ratio of the converter.

This paper proposes a new soft-switched CCM boost converter suitable for high-power applications such as power factor correction, hybrid electric vehicles, and fuel cell power conversion systems. The proposed converter has the following advantages:

- 1) ZVS turn-on of the main switches in CCM;
- 2) negligible diode reverse recovery due to ZCS turn-off of the diode;
- 3) voltage conversion ratio is almost doubled compared to the conventional boost converter;
- 4) significantly reduced components' voltage ratings and energy volumes of most passive components.

The operating principles and features of the proposed converter are described. Experimental results from a 1.5-kW prototype are also provided to validate the proposed concept.

II. PROPOSED SOFT-SWITCHED BOOST CONVERTER

Fig. 1 shows the circuit diagram of the proposed CCM boost converter, and Fig. 2 shows key waveforms illustrating the operating principle of the proposed converter. Upper switch S_2 in the proposed converter replaces the rectifier diode in the conventional boost converter. Lower switch S_1 and upper switch

Manuscript received July 27, 2009; revised September 15, 2009 and November 3, 2009. Current version published May 7, 2010. Recommended for publication by Associate Editor F. L. Luo.

S. Park is with the Research and Development Department, INTECH FA Company, Yongin-si 449-882, Korea (e-mail: sspark@intech-fa.co.kr).

S. Choi is with the Department of Control and Instrumentation Engineering, Seoul National University of Technology, Seoul 139-743, Korea (e-mail: schoi@snut.ac.kr).

Color versions of one or more of the figures in this paper are available online at <http://ieeexplore.ieee.org>.

Digital Object Identifier 10.1109/TPEL.2010.2040090

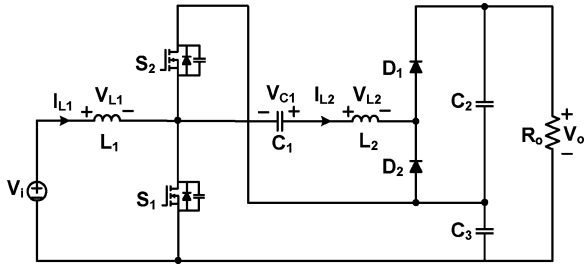


Fig. 1. Proposed soft-switched CCM boost converter.

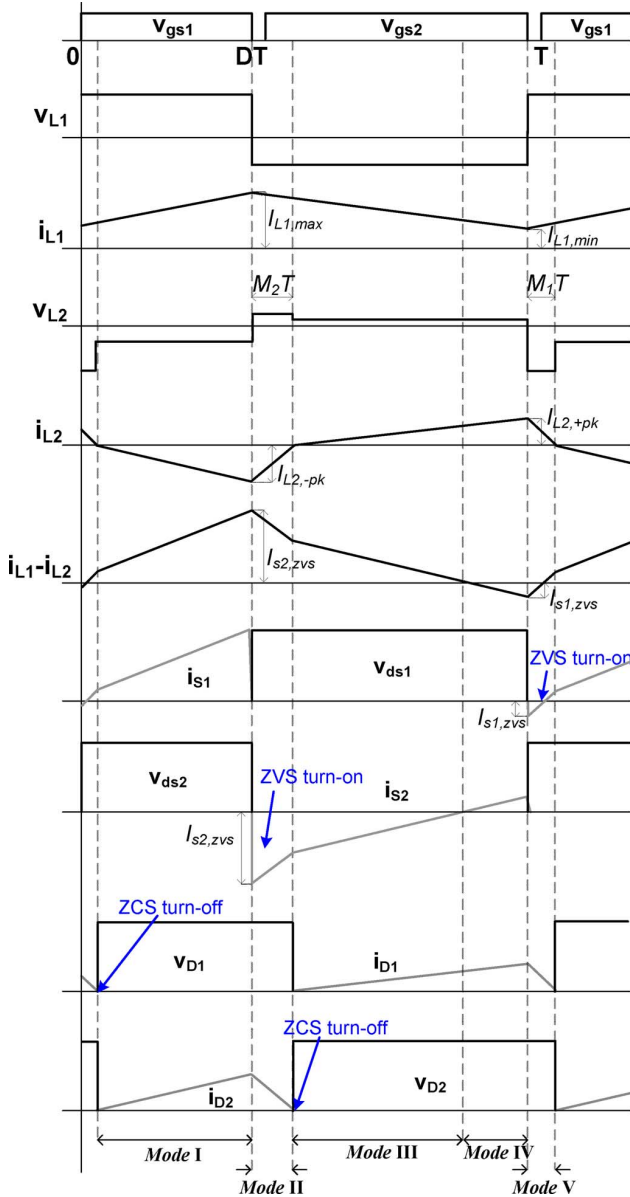


Fig. 2. Key waveforms of the proposed converter.

S_2 are operated with asymmetrical complementary switching to regulate the output voltage as shown in Fig. 2. An auxiliary circuit that consists of a capacitor C_1 , an inductor L_2 , two diodes D_1 and D_2 , and a capacitor C_2 is connected on top of the output capacitor C_3 to form the output voltage of the converter. The

auxiliary circuit not only increases the output voltage, but also helps ZVS turn-on of active switches S_1 and S_2 in CCM.

A. Operating Principle

As shown in Fig. 2, the operation of the proposed converter can be divided into five modes. The equivalent circuits for each mode are shown in Fig. 3.

Mode I: This mode begins when i_{L_2} decreases to zero and D_2 is turned on as shown in Fig. 2. During this mode, the lower switch S_1 maintains ON state. Both input inductor current i_{L_1} and auxiliary inductor current i_{L_2} flows through lower switch S_1 . The slope of these currents are given by

$$\frac{di_{L_1}}{dt} = \frac{V_i}{L_1} \quad (1)$$

$$\frac{di_{L_2}}{dt} = \frac{(V_{C_1} - V_{C_3})}{L_2}. \quad (2)$$

Mode II: This mode begins when S_1 is turned off and the body diode of S_2 is turned on. The gating signal for S_2 is applied during this mode, and S_2 is turned on under ZVS conditions. Both i_{L_1} and i_{L_2} are decreasing with the slope determined by the following equations:

$$\frac{di_{L_1}}{dt} = \frac{(V_i - V_{C_3})}{L_1} \quad (3)$$

$$\frac{di_{L_2}}{dt} = \frac{V_{C_1}}{L_2}. \quad (4)$$

At the end of this mode, inductor current i_{L_2} changes its direction of flow and D_1 starts to conduct. It should be noted that D_2 is turned off under ZCS.

Mode III: During this mode, i_{L_1} keeps decreasing with the slope determined in Mode II, and i_{L_2} increases with slope determined by the following equation:

$$\frac{di_{L_2}}{dt} = \frac{(V_{C_1} - V_{C_2})}{L_2}. \quad (5)$$

At the end of this mode, switch current i_{s_2} reverses its direction of flow and conducts the main channel of S_2 .

Mode IV: During this mode, i_{L_1} and i_{L_2} keep flowing with the same slope determined in Mode III.

Mode V: This mode begins when S_2 is turned off and the body diode of S_1 is turned on. The gating signal for S_1 is applied during this mode, and S_1 could be turned on under ZVS conditions. Inductor currents i_{L_1} and i_{L_2} start to increase and decrease, respectively, with the slope determined by the following equations:

$$\frac{di_{L_1}}{dt} = \frac{V_i}{L_1} \quad (6)$$

$$\frac{di_{L_2}}{dt} = \frac{V_{C_1} - V_{C_2} - V_{C_3}}{L_2}. \quad (7)$$

This state ends when the decreasing current i_{L_2} reaches to 0 V. This is the end of one complete cycle. Note that diode D_1 is also turned off under ZCS.

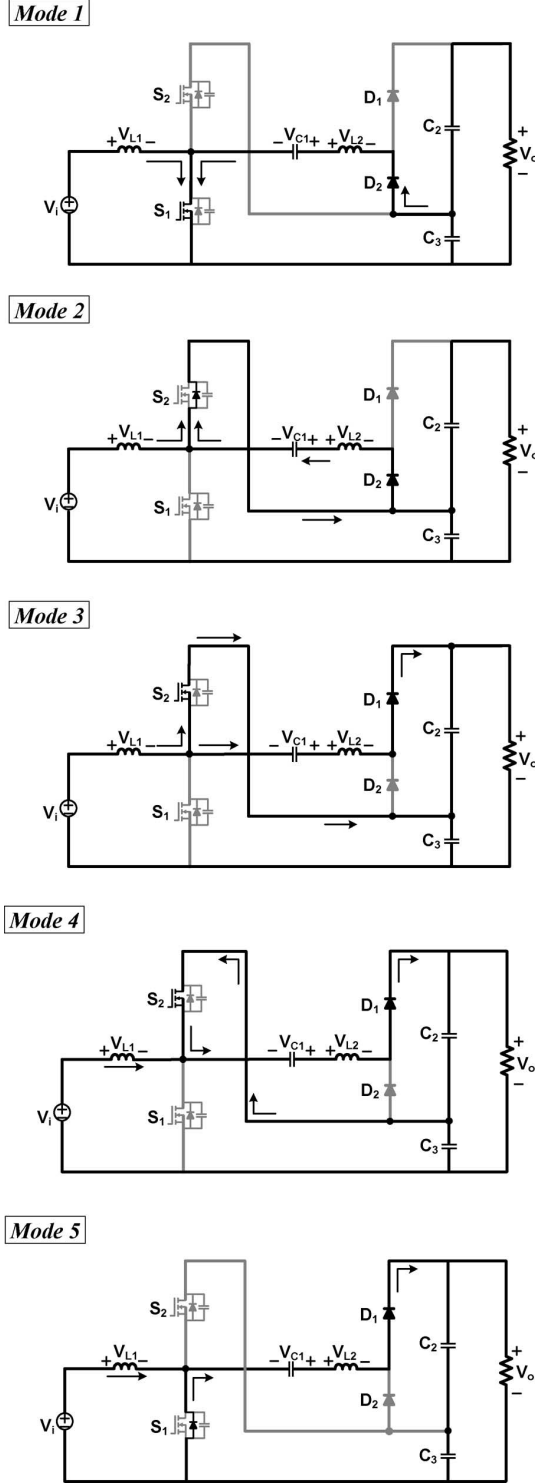


Fig. 3. Operation modes of the proposed converter.

B. Voltage Conversion Ratio

To obtain the voltage gain of the proposed converter, it is assumed that the voltage across C_1 , C_2 , and C_3 are constant during the switching period of T_S . The output voltage is given by

$$V_o = V_{C_2} + V_{C_3} \quad (8)$$

or

$$V_o = \frac{2}{1 - D_{\text{eff}}} V_i \quad (9)$$

where the effective duty D_{eff} is defined by

$$D_{\text{eff}} = D + M_1 - M_2. \quad (10)$$

The output voltage can also be expressed as

$$V_o = \frac{2}{1 - D} V_i - \Delta V \quad (11)$$

where ΔV is the voltage drop caused by the duty loss ($M_2 - M_1$). From (9)–(11), the voltage drop ΔV can be obtained by

$$\Delta V = \frac{2V_i(M_2 - M_1)}{(1 - D)(1 - D + M_2 - M_1)}. \quad (12)$$

According to volt-sec balance principle on L_2 , capacitor voltage V_{C_1} can be obtained by

$$V_{C_1} = V_{C_2}(1 - D - (M_2 - M_1)) + DV_{C_3} \quad (13)$$

where V_{C_2} and V_{C_3} can be expressed as

$$V_{C_3} = \frac{1}{1 - D} V_i \quad (14)$$

$$V_{C_2} = \frac{1}{1 - D} V_i - \Delta V. \quad (15)$$

In the steady state, the average output load current equals the average current of D_1 and D_2 since the average value of the current through L_2 (C_2) is zero. The following equations can be derived:

$$I_{D_1, \text{av}} = \frac{V_o}{R_o} = \frac{1}{2}(1 - D - (M_2 - M_1))I_{L_2, +\text{pk}} \quad (16)$$

$$I_{D_2, \text{av}} = \frac{V_o}{R_o} = \frac{1}{2}(D + M_2 - M_1)I_{L_2, -\text{pk}} \quad (17)$$

where $I_{L_2, +\text{pk}}$ and $I_{L_2, -\text{pk}}$ are positive and negative peak values of the inductor current I_{L_2} , and are given by (see Fig. 2)

$$I_{L_2, +\text{pk}} = \frac{(V_{C_1} - V_{C_2} - V_{C_3})M_1 T_S}{L_2} \quad (18)$$

$$I_{L_2, -\text{pk}} = \frac{V_{C_1} M_2 T_S}{L_2}. \quad (19)$$

Diode current I_{D_2} , which is a negative portion of current I_{L_2} , becomes incremental current in switch S_1 , resulting in increased conduction loss. At the same time, diode current I_{D_1} , which is a positive portion of current I_{L_2} , becomes decremental current in switch S_2 , resulting in decreased conduction loss.

Also, current I_{L_2} increases the ZVS currents for both lower switch, $I_{S_1, \text{ZVS}}$, and upper switch, $I_{S_2, \text{ZVS}}$, resulting in reduced switching losses. The peak values $I_{L_2, -\text{pk}}$ and $I_{L_2, +\text{pk}}$ can be adjusted by the inductance L_2 . Therefore, the magnitude of current I_{L_2} should be properly designed considering this tradeoff relation.

Using (11)–(19), the effective voltage gain of the proposed converter is plotted as shown in Fig. 4. Even though there is a slight drop of the ideal voltage gain, which is caused by duty loss ($M_2 - M_1$), the effective voltage gain of the proposed converter is almost twice compared to that of the conventional boost

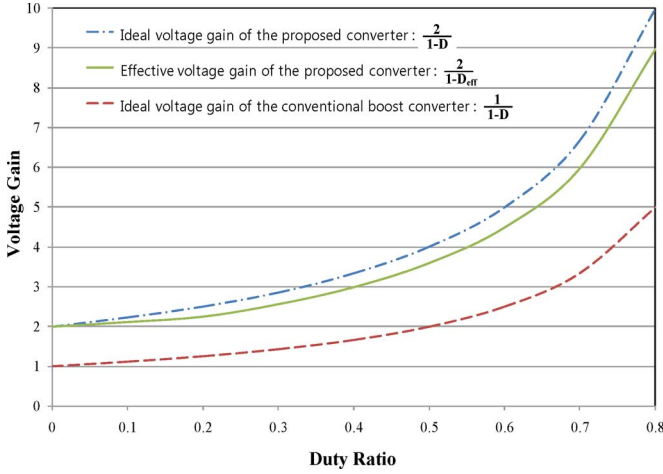


Fig. 4. Voltage gain as a function of duty ratio ($V_i = 80$ V, $L_2 = 7$ μ H, $f_s = 70$ kHz, $P_o = 1.5$ kW).

converter. This is a very desirable feature in high-voltage-gain application since reduced duty ratio leads to reduced current stresses on the components resulting in increased efficiency. Duty loss ($M_2 - M_1$) can be reduced by choosing smaller inductance L_2 , but this reduces ZVS range of main switch S_1 . Therefore, inductance L_2 should be properly chosen, considering a tradeoff of switching loss and voltage gain.

C. ZVS Characteristic for Main Switch

ZVS of the upper and lower switches depends on the difference of the filter inductor current i_{L_1} and auxiliary inductor current i_{L_2} , as shown in Fig. 2. The ZVS current for lower switch $I_{S_1,ZVS}$ is the positive peak of $i_{L_1} - i_{L_2}$ when the upper switch is turned off and can be expressed as

$$\begin{aligned} I_{S_1,ZVS} &= I_{L_2,+pk} - I_{L_1,min} \\ &= \frac{(V_{C_1} - V_{C_2} - V_{C_3})M_1T_s}{L_2} - \left(\frac{V_o^2}{V_i R_o} + \frac{DV_i}{2L_1 f_s} \right). \end{aligned} \quad (20)$$

The ZVS current for upper switch $I_{S_2,ZVS}$ is the negative peak of $i_{L_1} - i_{L_2}$ when the lower switch is turned off and can be expressed as

$$\begin{aligned} I_{S_2,ZVS} &= |I_{L_2,-pk}| + I_{L_1,max} \\ &= \frac{V_{C_1} M_2 T_s}{L_2} + \left(\frac{V_o^2}{V_i R_o} + \frac{DV_i}{2L_1 f_s} \right). \end{aligned} \quad (21)$$

To ensure the ZVS turn-on of upper switch S_2 , the following condition should be satisfied:

$$\frac{1}{2}(L_1 I_{L_1,max}^2 + L_2 I_{L_2,-pk}^2) > \frac{1}{2}(C_{os1} + C_{os2}) \left(\frac{V_i}{1-D} \right)^2 \quad (22)$$

where C_{os1} and C_{os2} are the output capacitances of lower switch S_1 and upper switch S_2 , respectively.

In fact, the condition of (22) can be easily satisfied, and ZVS of upper switch S_2 can be achieved over the whole load range. To ensure the ZVS turn-on of lower switch S_1 , the following

condition should be satisfied:

$$\frac{1}{2}(L_2 I_{L_2,+pk}^2 - L_1 I_{L_1,min}^2) > \frac{1}{2}(C_{os1} + C_{os2}) \left(\frac{V_i}{1-D} \right)^2. \quad (23)$$

Equation (23) may not be satisfied under the conditions of small auxiliary inductance L_2 , large input filter inductance L_1 , and/or light load. Increasing auxiliary inductance L_2 to enlarge the ZVS region makes the duty loss ($M_2 - M_1$) large. Alternatively, in order to enlarge the ZVS region, the input inductance can be decreased so that $I_{S_1,ZVS}$ can be increased. However, decreasing the input filter inductance increases the current rating of the power devices, and therefore the input filter inductance should be properly chosen considering a tradeoff between the ZVS region and the device current ratings. Therefore, ZVS for lower switch S_1 can be achieved more easily with smaller value of L_1 and/or larger value of L_2 at the cost of the large current ripple. A tradeoff of switching loss and conduction loss should be considered.

Using (20)–(23), the ZVS currents and ZVS ranges of lower and upper switches as the function of voltage gain and output power are plotted, respectively, as shown in Fig. 5. As shown in Fig. 5(a), the ZVS current of the lower switch tends to increase as the output power increases and decrease as the voltage gain increases. This means that the ZVS turn-on of the lower switch can be more easily achieved under the condition of higher output power and lower voltage gain. It is noted that the ZVS range of the lower switch becomes broader for smaller total output capacitance $C_{os,tot} = C_{os1} + C_{os2}$ of MOSFETs. For example, if MOSFETs with total output capacitance $C_{os,tot}$ of 1.8 nF are selected in this example, the ZVS turn-on of the lower switch can be achieved with output power that is greater than 500 W at voltage gain of 5 [see Fig. 5(a)].

The ZVS current of the upper switch also tends to increase as the output power and voltage gain increase. It should be noted from Fig. 5(b) that the ZVS turn-on of the upper switch can be achieved in the overall input voltage and output power ranges.

D. Comparison of Component Ratings

In order to perform a comparison of the proposed converter to the conventional ZVT converter [10] in terms of the component rating, the converters have been designed according to the following specifications:

- 1) $P_o = 13$ kW;
- 2) $V_i = 250$ V;
- 3) $V_o = 600$ V;
- 4) $\Delta I_i = 10\%$;
- 5) $\Delta V_o = 3\%$;
- 6) $f_s = 15$ kHz.

The component ratings of the proposed converter and the ZVT converter calculated according to the design specification are listed in Table I. Because of the proposed connection of the auxiliary circuit, the voltage ratings of all components of the proposed converter are much smaller compared to those of the ZVT converter that are the same as the output voltage. Therefore, the switch and diode utilizations of the proposed converter are greatly improved.

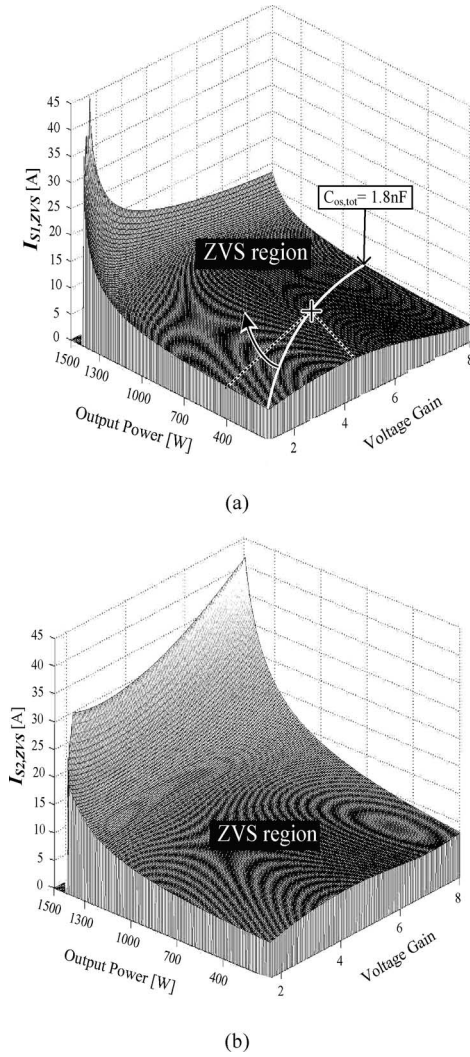


Fig. 5. ZVS currents and ZVS ranges of lower and upper switches as the function of the voltage gain and output power. (a) Lower switch S_1 . (b) Upper switch S_2 ($V_o = 400$ V, $P_o : 100\text{--}1.5$ kW, $L_2 = 7$ μ H, and $f_s = 70$ kHz).

Energy volume of the output capacitor of the proposed converter is slightly increased compared to the ZVT converter since two capacitors are required at the output. However, energy volumes of the other passive components are significantly reduced in the proposed converter. Input inductance of the proposed converter is smaller because the voltage across the inductor is smaller. Also, the current rating of the auxiliary inductor is much smaller compared to that of the ZVT converter, since the proposed converter does not utilize resonance while the ZVT converter utilizes partial resonance for soft switching.

III. EXTENSION OF THE PROPOSED CONCEPT

Using the converter shown in Fig. 1 as a basic cell, the proposed concept can be extended to realize multiphase dc–dc converters for high-voltage and high-power applications. Fig. 6 shows the generalized circuit of the proposed multiphase dc–dc converter. The generalized converter has “ N ” groups of converters, where each group of switch legs is connected in parallel

TABLE I
COMPARISON OF COMPONENT RATINGS OF THE PROPOSED CONVERTER AND THE ZVT CONVERTER

Components	Design Item	ZVT Converter[10]	Proposed Converter
Active Switches	V_{pk}	612 V	387 V
	I_{pk}	653 A	156 A
	$P_o / (V_{pk} \cdot I_{pk} \cdot q)$	0.02	0.11
Diodes	V_{pk}	612 V	223 V
	I_{pk}	52 A, 650A	101 A
	$P_o / (V_{pk} \cdot I_{pk} \cdot q)$	0.03	0.3
Output Capacitor	Capacitance	50 μ F	120 μ F x 2EA
	V_{pk}	612 V	223 V, 387 V
	$CV^2(\text{PU})$	1	1.3
Input Inductor	Inductance	1400 μ H	1200 μ H
	I_{rms}	52 A	52 A
	$LI^2(\text{PU})$	1	0.86
Auxiliary Capacitor	Capacitance	2 μ F	30 μ F
	I_{rms}	98 A	50 A
	V_{pk}	612 V	284 V
	$CV^2(\text{PU})$	1	3.2
Auxiliary Inductor	Inductance	2 μ H	25 μ H
	I_{rms}	277 A	50 A
	$LI^2(\text{PU})$	1	0.4

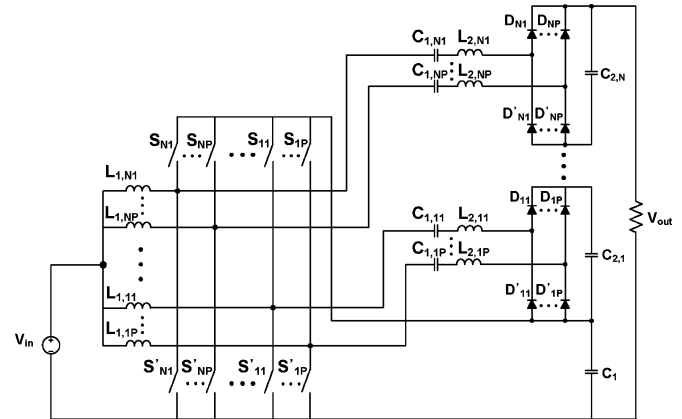


Fig. 6. Extension of the proposed concept for multiphase dc–dc converter (N is the number of series-connected output capacitors on top of C_1 and P is the number of diode legs connected to the same output capacitors).

at the low-voltage high-current side, while output capacitors in each group is connected in series at the high-voltage low-current side. Each of the N groups also has “ P ” parallel connected switch legs to increase the output power, where “ P ” is the number of switch or diode legs connected to the same output capacitor. That is to say, “ N ” could be increased to get higher output voltage and “ P ” could be increased to get higher output power.

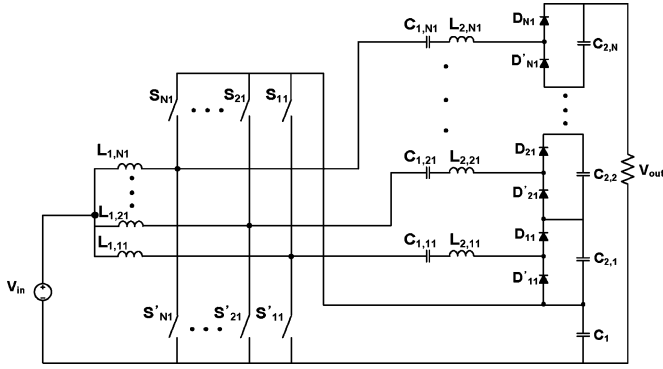


Fig. 7. Example circuit configuration of the proposed multiphase converter to increase the output voltage ($P = 1$).

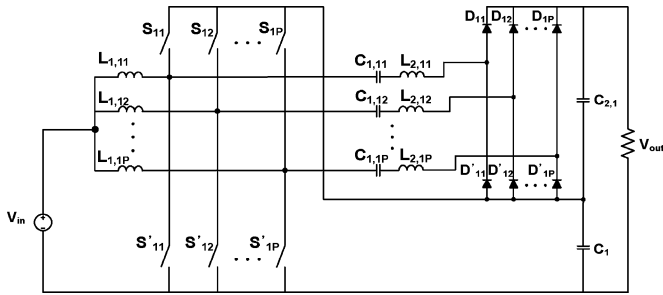


Fig. 8. Example circuit configuration of the proposed multiphase converter to increase the output power ($N = 1$).

Fig. 7 shows an example circuit configuration ($P = 1$), which illustrates how to increase output voltage by increasing “ N .” Fig. 8 shows an example circuit configuration ($N = 1$), which illustrates how to increase power level by increasing “ P .”

In both cases, the interleaving technique can be applied to reduce the size of input filter inductors, and input and output capacitors. Therefore, “ N ” and “ P ” could properly be chosen according to given output voltage and power level. This could give flexibility in device selection, resulting in optimized design even under harsh design specifications.

IV. EXPERIMENTAL RESULT

Using the previously designed parameters, a 1.5-kW soft-switched CCM boost converter prototype shown in Fig. 1 has been built in the laboratory.

- 1) $P_o = 1.5$ kW;
- 2) $V_i = 80$ V;
- 3) $V_o = 400$ V;
- 4) $\Delta I_i = 30\%$;
- 5) $\Delta V_o = 3\%$;
- 6) $f_s = 70$ kHz.

Both lower and upper switches are implemented with IXYS IXFN48N50 (500 V, 48 A, 1 m Ω) MOSFET. Fast recovery diodes of DAWIN Electronics DWM2F120N030 (300 V, 23 A) are used for diodes D_1 and D_2 . Input filter inductor L_1 and auxiliary inductor L_2 are 50 and 7 μ H, respectively. The designed values of the auxiliary capacitor C_1 is 50 μ F 200 V. An off-the-shelf electrolytic capacitor of 220 μ F 400 V was used

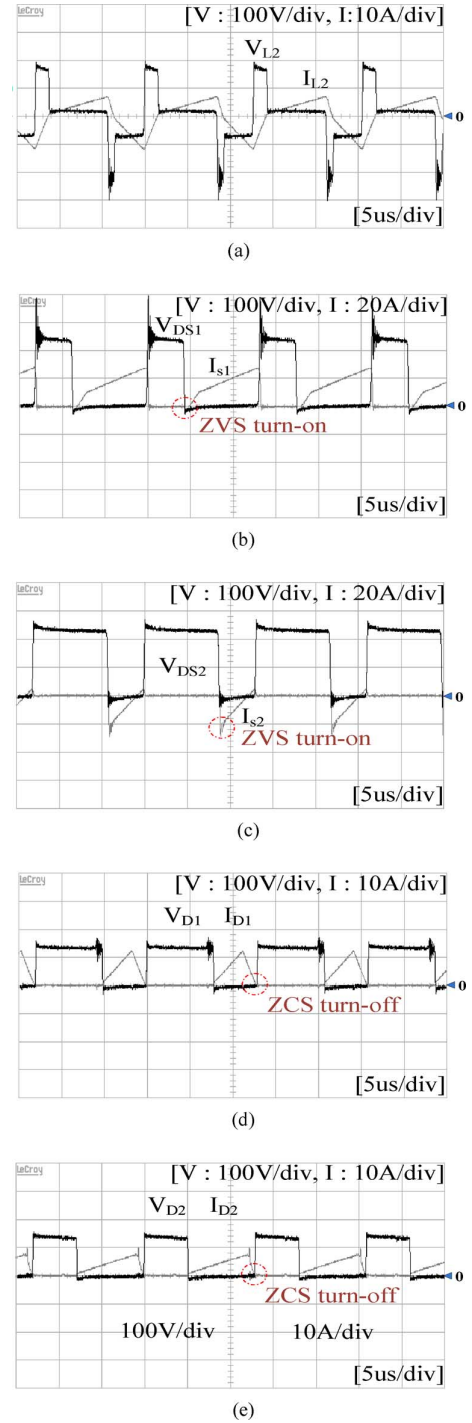


Fig. 9. Experimental waveforms. (a) Voltage and current waveforms of auxiliary inductor L_2 . (b) Voltage and current waveforms of lower switch S_1 . (c) Voltage and current waveforms of upper switch S_2 . (d) Voltage and current waveforms of upper diode D_1 . (e) Voltage and current waveforms of lower diode D_1 .

for C_1 since the rms value of ripple current is 6 A at 1.5 kW. Electrolytic capacitors of 220 μ F 400 V was also used for output capacitors C_2 and C_3 .

The experimental waveforms of the proposed scheme are shown in Fig. 9. Fig. 9 (a) shows voltage and current waveforms of auxiliary inductor L_2 . Fig. 9 (c) and (d) illustrates that both

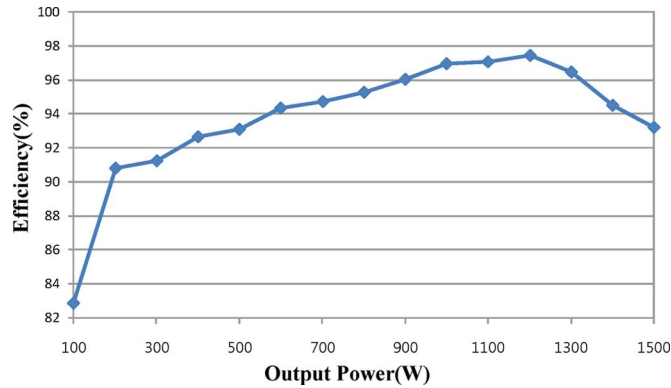


Fig. 10. Measured efficiency of the proposed converter.

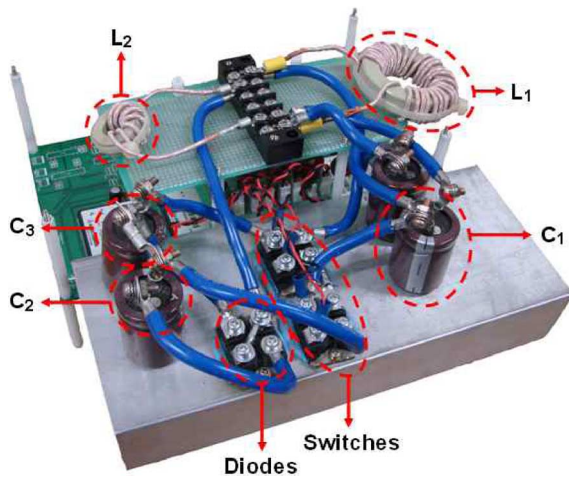


Fig. 11. Photograph of 1.5-kW soft-switched CCM boost converter prototype.

switch S_1 and switch S_2 are being turned on with ZVS. Fig. 9(d) and (e) shows that diodes D_1 and D_2 are being turned off with ZCS. The measured efficiency is shown in Fig. 10. The efficiency of the proposed converter maintains over 90% in most of the load range. The maximum efficiency of 97.4% was measured at 1200 W load. Fig. 11 shows the photograph of the prototype.

V. CONCLUSION

In this paper, a new soft-switched CCM boost converter suitable for high-voltage and high-power application has been proposed. The proposed converter has the following advantages:

- 1) ZVS turn-on of the active switches in CCM;
- 2) negligible diode reverse recovery due to ZCS turn-off of the diodes;
- 3) voltage conversion ratio is almost doubled compared to the conventional boost converter;
- 4) greatly reduced components' voltage ratings and energy volumes of most passive components.

Extension of the proposed concept to realize multiphase dc-dc converters for higher voltage and higher power applications has been explored. Experimental waveforms from a 1.5-kW prototype have been provided and peak efficiency of 97.4% was measured at 1200 W.

REFERENCES

- [1] C. Wang, M. H. Nehrir, and H. Gao, "Control of PEM fuel cell distributed generation systems," *IEEE Trans. Energy Convers.*, vol. 21, no. 2, pp. 586–595, Jun. 2006.
- [2] K. Liu, R. Oruganti, and F. C. Lee, "Resonant switched-topologies and characteristics," *IEEE Trans. Power Electron.*, vol. PE-2, no. 1, pp. 62–74, Jan. 1987.
- [3] V. Vorperian, "Quasi-square-wave converters: Topologies and analysis," *IEEE Trans. Power Electron.*, vol. 3, no. 2, pp. 183–191, Apr. 1988.
- [4] G. Hua, E. X. Yang, Y. Jiang, and F. C. Lee, "Novel zero-current-transition PWM converters," *IEEE Trans. Power Electron.*, vol. 9, no. 6, pp. 601–606, Nov. 1994.
- [5] Q. Zhao, P. Xu, and F. C. Lee, "A simple and effective method to alleviate the rectifier reverse-recovery problem in continuous-current-mode boost converters," *IEEE Trans. Power Electron.*, vol. 16, no. 5, pp. 649–658, Sep. 2001.
- [6] A. Ostadi, X. Gao, and G. Moschopoulos, "Circuit properties of zero-voltage-transition PWM converters," *J. Power Electron.*, vol. 8, no. 1, pp. 35–50, Jan. 2008.
- [7] B. duk Min, J. P. Lee, and E. H. Song, "A novel grid-connected PV PCS with new high efficiency converter," *J. Power Electron.*, vol. 8, no. 4, pp. 309–316, Oct. 2008.
- [8] M. S. Elmore, "Input current ripple cancellation in synchronized, parallel connected critically continuous boost converters," in *Proc. IEEE APEC*, 1996, pp. 152–158.
- [9] B. Eckardt, A. Hofmann, and S. Zeltner, "Automotive powertrain DC/DC converter with 25 kW. dm3 by using SiC diodes," presented at the ECPE CIPS Conf., Nuremberg, Germany, Mar. 2008.
- [10] T. Mizoguchi, T. Ohgai, and T. Ninomiya, "A family of single-switch ZVS-CV DC–DC converters," in *Proc. IEEE APEC*, 1994, vol. 2, pp. 1392–1398.
- [11] E. Ismail and A. Sebzali, "A new class of quasi-square wave resonant converters with ZCS," in *Proc. IEEE APEC*, 1997, pp. 1381–1387.
- [12] G. Hua, C. Leu, and F. C. Lee, "Novel zero-voltage-transition PWM converters," in *Proc. IEEE PESC*, 1992, pp. 55–61.
- [13] C. Kim, G. Moon, and S. Han, "Voltage doubler rectified boost-integrated half bridge (VDRBHB) converter for digital car audio amplifiers," *IEEE Trans. Power Electron.*, vol. 22, no. 6, pp. 2321–2330, Nov. 2007.
- [14] Y.-C. Hsieh, T.-C. Hsueh, and H.-C. Yen, "An interleaved boost converter with zero-voltage transition," *IEEE Trans. Power Electron.*, vol. 24, no. 4, pp. 973–978, Apr. 2009.
- [15] Q. Li and P. Wolfs, "An analysis of the ZVS two-inductor boost converter under variable frequency operation," *IEEE Trans. Power Electron.*, vol. 22, no. 1, pp. 120–131, Jan. 2007.



Sungsik Park was born in Incheon, Korea, in 1984. He received the B.S. and M.S. degrees from the Department of Control and Instrumentation Engineering, Seoul National University of Technology, Seoul, Korea, in 2007 and 2009, respectively.

He is currently an Engineer of the Research and Development Department, INTECH FA Company, Yongin, Korea. His research interests include high-power dc-dc converter and power conversion technologies in renewable energy systems.



Sewan Choi (S'92–M'96–SM'04) received the B.S. degree in electronic engineering from Inha University, Incheon, Korea, in 1985, and the M.S. and Ph.D. degrees in electrical engineering from Texas A&M University, College Station, in 1992 and 1995, respectively.

From 1985 to 1990, he was with Daewoo Heavy Industries as a Research Engineer. From 1996 to 1997, he was a Principal Research Engineer at Samsung Electro-Mechanics Company, Korea. In 1997, he joined the Department of Control and Instrumentation Engineering, Seoul National University of Technology, Seoul, Korea, where he is currently a Professor. His research interests include three-phase power factor correction, power conversion technologies in renewable energy systems, and dc-dc converters for hybrid electric and fuel cell vehicles.

Prof. Choi is an Associate Editor of the *IEEE TRANSACTIONS ON POWER ELECTRONICS* and the *IEEE TRANSACTIONS ON INDUSTRY APPLICATIONS*.